PHYSICAL REVIEW A VOLUME 25, NUMBER 5 MAY 1982

Collision kernels and laser spectroscopy

P. R. Berman
Physics Department, New York University, 4 Washington Place, New York, New York 10003

T. W. Mossberg
Department of Physics, Harvard University, Cambridge, Massachusetts 02138

S. R. Hartmann
Columbia Radiation Laboratory, Department of Physics, Columbia University, New York, New York 10027

(Received 24 August 1981)

Collisional processes occurring within an atomic vapor can be conveniently described in terms of collision kernels. The population kernel $W_{ii}(\vec{v}' \rightarrow \vec{v})$ gives the probability density per unit time that an "active" atom in state i undergoes a collision with a perturber that changes the active atom's velocity from $\vec{v}'$ to $\vec{v}$. For active atoms in a linear superposition of states i and j, there is an analogous *coherence kernel* $W_{ij}(\vec{v}' \rightarrow \vec{v})$ $(i \neq j)$ reflecting the effects of collisions on the off-diagonal density-matrix element ρ_{ij}. In this work, we discuss the general properties of the collision kernels which characterize a two-level active atom which, owing to the action of a radiation field, is in a linear superposition of its two levels. Using arguments based on the uncertainty principle, we show that collisions can be divided roughly into the following two categories: (1) collisions having impact parameters less than some characteristic radius which may be described classically and (2) collisions having impact parameters larger than this characteristic radius which give rise to diffractive scattering and must be treated using a quantum-mechanical theory. For the population kernels, collisions of type (1) can lead to a large-angle scattering component, while those of type (2) lead to a small-angle (diffractive) scattering component. For the coherence kernel, however, assuming that the collisional interaction for states i and j differ appreciably, only collisions of type (2) contribute, and the coherence kernel contains a small-angle scattering component only. The absence of a large-angle scattering component in the coherence kernel is linked to a collision-induced spatial separation of the trajectories associated with states i and j. Interestingly enough, the width of the diffractive kernel, as measured in the laboratory frame, is found to be insensitive to the perturber to active-atom mass ratio. To illustrate these features, a specific calculation of the kernels is carried out using a hard-sphere model for the scattering. The relationship of the present description of collisions to that of traditional pressure-broadening theory in which trajectory separation effects are ignored is discussed. It is explained why traditional pressure-broadening theory correctly describes collision effects in linear spectroscopy, but fails to provide an adequate description of some saturation spectroscopy and photon-echo experiments in which velocity-changing collisions associated with the coherence kernel play a significant role. An expression for the collisionally modified photon-echo amplitude is derived which clearly displays the role played by velocity-changing collisions associated with the coherence kernel.

I. INTRODUCTION

Emission and absorption spectra have traditionally provided the blueprints from which most of our data concerning the energy-level structure of atoms and molecules could be derived. The precision of this data is limited by one's inability to resolve structure that lies within the widths of the various spectral lines. In low-density atomic vapors, the linewidth is determined mainly by the Doppler effect (i.e., atoms moving at different velocities absorb or emit Doppler-shifted frequencies), although both the natural widths of the levels and collisions within the vapor contribute somewhat. One of the most exciting achievements in spectroscopy over the last decade has been the

development of methods wherein the Doppler width is partially or totally suppressed. The development of these "Doppler-free" methods in both time (e.g., photon-echo) and frequency (e.g., saturation spectroscopy) domain experiments has been made possible in large part by the advances in laser technology. With the removal of the Doppler broadening, the line shapes increasingly reflect the effects of collisional processes occurring in the vapor. It is not surprising, therefore, that the progress in laser spectroscopy has been accompanied by a renewed interest in understanding (1) the manner in which collisions modify the line shapes and (2) the extent to which laser spectroscopy can be used as a probe of collisional processes in vapors.

In order to illustrate the role played by collisions in atomic spectroscopy, we consider an ensemble of two-level "active" atoms immersed in a low-density vapor of "perturber" atoms. The levels of each active atom (labeled 1 and 2) are coupled by a radiation field. The active atoms undergo binary collisions with the perturbers (active-atom—active-atom collisions are neglected). The collisions are assumed to be adiabatic in the sense that they possess insufficient energy to induce transitions between the active-atom's levels. Under these conditions, one may seek to determine the manner in which these elastic collisions affect the physical observables associated with the active atoms.

The problem can be approached by investigating in detail a collision between an active atom and a perturber (Fig. 1). The active atom, which is prepared in a linear superposition of its two levels by a radiation field, generally experiences a collisional interaction which is different for states 1 and 2. From a classical viewpoint, the collisional interaction (acting analogously to a Stern-Gerlach magnet) separates the populations (conveniently represented by density matrix elements ρ_{11} and ρ_{22}) along the distinct trajectories shown in Fig. 1. Since the populations scatter independently, the

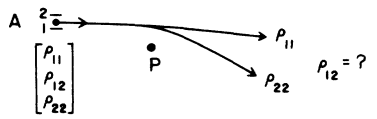

FIG. 1. Picture of a collision between an active atom A and stationary perturber P. There is no obvious classical trajectory to associate with the atomic "coherence" ρ_{12}.

possibility of distinct post-collision trajectories poses no conceptual difficulties. The scattering for each state i ($i=1,2$) is determined by the differential cross section $\sigma_i(\theta) = |f_i(\theta)|^2$ for the elastic scattering of an active atom in state i by a perturber atom.[1]

The populations ρ_{ii}, however, are not the only relevant quantities in considering the interaction of radiation with matter. The polarization of the vapor directly influences its absorptive and dispersive properties. If the dipole moment operator of our two-level atom is $\hat{\mu}$ and if states 1 and 2 have opposite parity, then the polarization of the system is proportional to $\langle\hat{\mu}\rangle = \vec{\mu}_{12}\rho_{21} + \vec{\mu}_{21}\rho_{12}$, where $\vec{\mu}_{ij}$ is the ij matrix element of $\hat{\mu}$ and ρ_{ij} is the ij density-matrix element (i.e., $\rho_{ij} = a_i a_j^*$, where a_i is the state i probability amplitude). Consequently, the absorptive and dispersive properties of the medium are influenced by collisional perturbations of the "atomic coherence" ρ_{12} (or ρ_{21}).

Collisions appear to affect ρ_{12} in a particularly simple way. Since the collision shown in Fig. 1 leads to a spatial separation of states 1 and 2, ρ_{12} vanishes following the collision. Thus, using a classical picture of a collision, one is led to distinct trajectories for the populations ρ_{11} and ρ_{22} and to a vanishing of the coherence ρ_{12}.

While the classical picture of a collision given in Fig. 1 is useful in providing some insight into the effects of collisions on the various density-matrix elements, it is not sufficient to obtain a total picture of the scattering. Using arguments based on the uncertainty principle, we will show that, within certain limits, the classical picture is valid for small-impact parameter collisions. However, for large-impact parameter collisions, the quantum theory must be used. Quantum-mechanical effects give rise to diffractive scattering contributions for the populations and to nonvanishing values of ρ_{12} following a collision.

The discussion of a single collision given above would be appropriate to a crossed atomic-beam experiment in which the center-of-mass energy is constant for all collisions. In an atomic vapor, however, the perturbers have some velocity distribution which must be averaged over. For the vapor, the quantity of interest is the collision kernel $W_{ii}(\vec{v}' \to \vec{v})$ giving the probability density per unit time that an active atom in state i changes its velocity from $\vec{v}'$ to $\vec{v}$ in undergoing a collision with a perturber. The corresponding rate for such collisions is denoted by $\Gamma_i(\vec{v}')$. The kernel is proportional to the differential scattering cross section

averaged over the perturber velocity distribution consistent with conservation of momentum and energy. For off-diagonal density-matrix elements, one can also define a "kernel" $W_{12}(\vec{v}'\rightarrow\vec{v})$ and "rate" $\Gamma_{12}^{vc}(\vec{v}')$, although these quantities, now dependent on $f_1 f_2^*$, need no longer be positive definite. Formal expressions for $W_{12}(\vec{v}'\rightarrow\vec{v})$ and $\Gamma_{12}^{vc}(\vec{v}')$ have been given,[2,3] but there has been, with two recent exceptions,[4,5] little progress in obtaining a satisfactory physical interpretation or actual evaluation of the "coherence kernel" $W_{12}(\vec{v}'\rightarrow\vec{v})$.[6] It is the purpose of this paper to provide a simple physical picture of the scattering process that leads to an intuitive understanding of the nature of $W_{12}(\vec{v}'\rightarrow\vec{v})$.

It has already been noted that collisional perturbations of ρ_{12} affect the absorptive properties of a medium. Thus, one might imagine that collision induced modifications of absorption or emission line shapes are intimately connected with the coherence kernel $W_{12}(\vec{v}'\rightarrow\vec{v})$. Since $W_{12}(\vec{v}'\rightarrow\vec{v})$ is strongly influenced by the trajectory effects shown in Fig. 1, it appears that such trajectory effects are critical in calculating the effects of collisions on spectral line shapes. However, it is well known that traditional theories of pressure broadening,[7] which totally ignore trajectory effects of the type shown in Fig. 1 and consider collisions to produce only phase changes in ρ_{12}, have been very successful in explaining most spectral profiles. How, one may ask, can a theory that ignores trajectory separation effects still produce correct results? It is a second purpose of this paper to provide an answer to this question.

[There *is* a range of experimental situations where trajectory effects are known to be important.[8] In such experiments, however, the states involved in the transition (usually vibrational, rotational, or rf transitions) experience nearly identical collisional interactions and, consequently, follow the *same* collisional trajectory. Trajectory effects lead to a *narrowing* of spectral lines in linear spectroscopy and to a signal with a unique signature in photon-echo experiments.[9] In this paper, however, we shall be concerned only with situations where the collisional interaction for states 1 and 2 differs somewhat (the precise conditions are given below) as is generally the case for electronic transitions. Only recently has an experiment been performed that clearly indicates the importance of trajectory effects for an electronic transition.[10,11]]

In Sec. II, the uncertainty principle is used to obtain a simple physical picture of the scattering. It is shown that collisions can be divided roughly into two regions. For small-impact parameter collisions, the scattering can be given a classical interpretation; the distinct trajectories for states 1 and 2 shown in Fig. 1 then lead to a vanishing of ρ_{12} following the collision. On the other hand, for large-impact parameter collisions (leading to diffractive scattering), the classical picture fails and a quantum-mechanical calculation of ρ_{12} is needed. A specific evaluation of the coherence kernel and rates is made in Sec. III using a model potential based on hard-sphere scattering. The various features discussed in Sec. II are illustrated by this example. In Sec. IV, the role that the coherence kernel plays in affecting various spectroscopic line shapes is discussed. The reason for the success of traditional pressure-broadening theories is explained in this section. Finally, a calculation of a collisionally modified photon-echo signal is given in Sec. V. The role played by trajectory effects is clearly reflected in the expression for the echo amplitude.

For simplicity, the calculations carried out in Secs. II—V are made assuming a high ratio of perturber to active atom mass. In Appendix A, the calculations are extended to allow for an arbitrary mass ratio. It is shown that *the width of the coherence kernel is effectively independent of the ratio of perturber to active-atom mass* and depends only on the active-atom mass and collision cross section.

It is implicitly assumed throughout this work that an *impact approximation* is valid. All relevant frequencies (e.g., collision rates, atom-field detunings, Rabi frequencies) are assumed to be small in comparison with the inverse duration time of a collision. The validity of the impact approximation implies that only binary collisions need be considered and that these collisions produce a time rate of change for ρ_{ij} which is independent of other contributions to $\partial\rho_{ij}/\partial t$.

II. QUALITATIVE PICTURE OF SCATTERING

Before discussing the effects of collisions on ρ_{12} and the corresponding coherence kernel $W_{12}(\vec{v}'\rightarrow\vec{v})$, it is instructive to review some aspects of elastic scattering theory. Thus, we shall first consider the elastic scattering of an active atom in state i. To simplify the discussion we take the perturber as stationary (ratio of perturber to active-atom mass much greater than unity), but the results of this section are perfectly general if all vari-

ables are taken as those in the center-of-mass system. Moreover, we neglect such effects as orbiting, rainbow, and glory scattering which, although important in certain cases,[12] are not particularly relevent to the subject matter at hand.

A. Population kernel

The regions of validity of a classical picture of scattering can be established by using the uncertainty principle. Consider a collision characterized by an impact parameter b leading to scattering at an angle θ. For a classical picture to be valid, one must have

$$\Delta b < b, \quad \Delta\theta < \theta , \tag{1}$$

where Δb and $\Delta\theta$ are the uncertainties in b and θ, respectively. On the other hand, it follows from the uncertainty principle that $\Delta p_t \Delta b \gtrsim \hbar$, where Δp_t is the uncertainty in the transverse component of the active atom's momentum. Since $\Delta p_t \equiv m\Delta v_t \approx mv\Delta\theta = \hbar k\Delta\theta$ [m is the active-atom mass, $k \equiv mv/\hbar$, and v is the active-atom speed], the uncertainty principle requires that

$$k\Delta b\Delta\theta \gtrsim 1 . \tag{2}$$

Setting $\Delta b = b$ and $\Delta\theta = \theta$, one sees that conditions (1) and (2) can both be satisfied provided

$$\theta >> 1/(kb) . \tag{3}$$

Let b_i represent some characteristic range for scattering by the perturber of active atoms in the state i. For typical interaction potentials, it follows that a classical description of the scattering is valid if

$$\theta >> \theta_i^d \equiv 1/(kb_i) . \tag{4}$$

In fact, it is well known[12] that the quantum-mechanical expression for the differential scattering cross section reduces to the corresponding classical one if condition (4) is satisfied (neglecting any effects of rainbow scattering). Clearly, Eq. (4) is meaningful only if $kb_i > 1$.

On the other hand, for $\theta < \theta_i^d$ one can no longer expect the classical picture of scattering to remain appropriate. In an atomic vapor, k is typically of order 10^9 cm^{-1} and b_i is of order 10 Å so that $\theta_i^d \approx 0.01 << 1$. In effect, the angle θ_i^d separates the scattering into two distinct regions. For $\theta >> \theta_i^d$ (corresponding to collisions having $b < b_i$), the scattering may be described classically. For $\theta << \theta_i^d$ (corresponding to collisions having $b > b_i$) the scattering may be considered diffractive in nature and must be described quantum mechanically. [For other than purely repulsive potentials, the $\theta < \theta_i^d$ region also has (relatively weak) contributions from some collisions having $b < b_i$ ("glory scattering").[12] As noted earlier, effects such as orbiting or rainbow and glory scattering are neglected in this work.]

The above results imply that the collision kernel for elastic scattering in state i can be written as the sum of two terms corresponding to classical large-angle scattering and quantum-mechanical diffractive scattering, respectively.[13] There is recent experimental evidence that supports this conclusion.[14]

B. Coherence kernel

We are now in a position to discuss the effects of a collision on ρ_{12}. The interaction potential is assumed to be state dependent and it is further assumed that there are two characteristic lengths b_1 and b_2 associated with the scattering for states 1 and 2, respectively. For the sake of definiteness, we take $b_2 > b_1$. The question to be answered is the following: For what scattering angles, if any, may a classical picture be used to describe the effects of the scattering on ρ_{12}?

The question must first be clarified since the criterion we shall use to judge the validity of a classical picture is different than that used in the case of single-state elastic scattering. Scattering for ρ_{12} will be classified as "classical" if the trajectories associated with the elastic scattering from states 1 and 2 are distinct and nonoverlapping (see Fig. 1). A consequence of this classification is that ρ_{12} is zero following any classically described collision, since the spatial overlap of states 1 and 2 vanishes as a result of the collision.

An uncertainty principle argument can once again be used to obtain the classical region. Let θ_1 and θ_2 be the scattering angles associated with states 1 and 2 for a collision having impact parameter b. The criterion for a classical collision is then

$$\Delta b < b; \quad \Delta\theta < |\theta_2 - \theta_1| , \tag{5}$$

where $\Delta\theta$ is the uncertainty in θ for a collision with impact parameter b. The restriction imposed by the uncertainty principle is still given by Eq. (2), which may be combined with Eq. (5) to give

$$|\theta_2 - \theta_1| > 1/(kb) \tag{6}$$

as the distinct trajectory condition.

Equation (6) can be given a very interesting interpretation in terms of a parameter appearing in conventional theories of pressure broadening. An active atom in state i sees a potential $V(r)$ produced by a perturber, where r is the active-atom—perturber separation. The scattering angle θ_i, calculated assuming small-angle scattering, is

$$\theta_i = v_t/v \simeq -\frac{1}{\hbar k}\int \frac{\partial V_i(r)}{\partial b}dt \ , \tag{7}$$

where the integral is along the time parameterized collision trajectory $r(b,v,t)$. Setting $\partial V_i/\partial b = -\kappa b^{-1}V_i$ (κ is the constant of order unity) and substituting Eq. (7) into (6), one obtains the distinct trajectory condition[15]

$$\frac{1}{\hbar}\left|\int [V_2(b,t)-V_1(b,t)]dt\right| > \kappa^{-1} \simeq 1 \ . \tag{8}$$

The value of b, denoted by b_W, for which the left-hand side of Eq. (8) equals unity is the Weisskopf radius of pressure-broadening theory.[7] Equation (8) implies that the maximum impact parameter for which the distinct trajectory condition holds is $b \simeq b_W$; consequently, Eq. (6) is valid only for

$$b < b_W \tag{9}$$

(distinct trajectory condition). The consistency of the entire approach requires that

$$kb_W >> 1 \ . \tag{10}$$

One is led to the following result. For scattering angles corresponding to collisions having an impact parameter $b < b_W$, a classical picture is possible provided that Eq. (10) is valid. These classical collisions result in a complete destruction of ρ_{12} owing to the separation of trajectories for states 1 and 2. For diffractive scattering, corresponding to collisions having impact parameters $b > b_W$, a quantum-mechanical calculation is needed. In this case, ρ_{12} does not vanish following the collision (see Fig. 2). [Notice that the impact parameter separating the classical and quantum scattering domains differs somewhat for the populations and the coherences. The b_i associated with the populations may be calculated using Eqs. (3), (4), and (7).]

If $kb_W < 1$, a quantum-mechanical approach is needed for all scattering angles. In this limit the scattering is almost identical for states 1 and 2 ($b_W = 0$ for state-independent scattering) and there is non-negligible spatial overlap of the state 1 and 2 trajectories. In this work, we assume that the interaction potentials for the two levels differ sufficiently to insure that Eq. (10) holds for most atoms in the vapor. Typically $b_W \approx 5-10$ Å for electronic transitions so that $kb_W \approx 100 >> 1$.

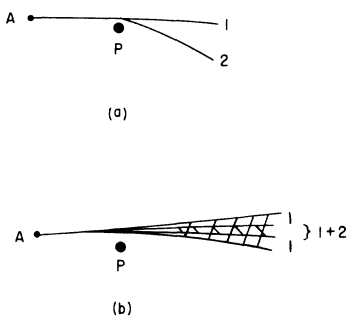

FIG. 2. Effects of collisions on ρ_{12} can be *roughly* visualized as shown in this figure when $kb_W = b_W/\lambda\!\!\!^{-} >> 1$. For collisions having impact parameter $b < b_W$ (a), the trajectories for states 1 and 2 are distinct and nonoverlapping following the collision, leading to a destruction of ρ_{12}. For collisions with $b > b_W$ (b), scattering is diffractive in nature. The overlap of the diffractive scattering cones for states 1 and 2 leads to nondestructive velocity-changing collisions associated with ρ_{12}.

The qualitative structure of the coherence kernel $W_{12}(\vec{v}' \to \vec{v})$ is now evident. In contrast to the population kernels, the coherence kernel *vanishes* in the large-angle scattering region owing to the separation of trajectory effects. For diffractive scattering, a quantum-mechanical calculation of $W_{12}(\vec{v}' \to \vec{v})$ is needed. Thus, the coherence kernel is effectively nonzero for diffractive scattering only. The consequences of this conclusion are discussed in Sec. IV.

In this section, a qualitative picture of the scattering process was given. In Sec. III, a coherence kernel is explicitly calculated assuming a simple form for the interaction potential. The calculation serves to illustrate the various features discussed in this section. The reader not interested in the details of the model-potential calculation can proceed to Sec. IV without loss of continuity.

III. MODEL-POTENTIAL CALCULATION

The qualitative properties of the collision kernels discussed in Sec. II are relatively insensitive to the form of the interaction potential. Therefore, for the sake of simplicity, we assume that the state i scattering potential can be represented as an impenetrable sphere of radius b_i (with $b_2 > b_1$). It should be noted, however, that the calculations presented below may easily be generalized to spherically symmetric potentials of an arbitrary nature.

To further simplify the calculations, we assume that the perturber is stationary, although a generalization of the results of this section to allow for an arbitrary active-atom-to-perturber-mass ratio is given in Appendix A. This section is organized as follows: A. The scattering amplitude for hard-sphere scattering is given and an exponential approximation to it, valid for diffractive scattering, is obtained. B. The collision kernel $W_{ii}(\vec{v}'\rightarrow\vec{v})$ and the rate $\Gamma_i(\vec{v})$ for this scattering of populations are calculated. C. The coherence kernel $W_{12}(\vec{v}'\rightarrow\vec{v})$ and the rate $\Gamma_{12}^{vc}(\vec{v})$ are evaluated. D. The coherence kernel and the rate are averaged over a transverse velocity distribution to obtain a one-dimensional kernel $W_{12}(\vec{v}_z'\rightarrow\vec{v}_z)$ and rate $\Gamma_{12}^{vc}(v_z)$ that appear in theories of laser spectroscopy.

A. Scattering amplitude

The scattering amplitude for elastic scattering of an active atom in state j by the perturber is

$$f_j(\theta)=\frac{1}{ik}\sum_{l=0}^{\infty}(l+\tfrac{1}{2})(e^{2i\eta_l^j}-1)P_l(\cos\theta)\ , \tag{11}$$

where the η_l^j are the elastic scattering phase shifts. For hard-sphere scattering, the η_l^j are equal to

$$\tan^{-1}[j_l(kb_j)/n_l(kb_j)]\ ,$$

where j_l and n_l are spherical Bessel and Neumann functions, respectively.

If $\theta>>(1/kb_j)^{1/3}$ (classical region), a standard calculation using the method of stationary phase gives[12,16]

$$f_j(\theta)=-(b_j/2)e^{i\phi_j(\theta)},\quad \theta>>(kb_j)^{-1/3} \tag{12a}$$

where

$$\phi_j(\theta)=-2kb_j\sin\frac{\theta}{2}\ . \tag{12b}$$

The differential cross section $|f_j(\theta)|^2=b_j^2/4$ is just the classical result for hard-sphere scattering. Thus, for $\theta>>(kb_j)^{-1/3}$, one regains the classical result, in agreement with the qualitative discussion of Sec. II.

For small-angle scattering $\theta<<1$, one can replace $P_l(\cos\theta)$ by the zero-order Bessel function $J_0((l+\frac{1}{2})\theta)$.[17] With this substitution, Eq. (11) becomes

$$f_j(\theta)=\frac{1}{ik}\sum_{l=0}^{\infty}(l+\tfrac{1}{2})(e^{2i\eta_l^j}-1)J_0((l+\tfrac{1}{2})\theta)\ . \tag{13}$$

Using some simple properties of the spherical Bessel functions, one can show that η_l^j is large and varies linearly with l for $l<L_j\equiv kb_j$ and that $\eta_l^j\rightarrow 0$ very rapidly for $l>L_j$. Thus, for $l<L_j$ the term containing $e^{2i\eta_l^j}$ varies rapidly and averages to zero (there is no point of stationary phase[18]) while, for $l>L_j$, $(e^{2i\eta_l^j}-1)\approx 0$. Equation (13) may then be approximated by[19]

$$f_j(\theta)\approx(i/k)\sum_{l=0}^{L_j}(l+\tfrac{1}{2})J_0((l+\tfrac{1}{2})\theta)\ . \tag{14}$$

By transforming the sum (14) into an integral, one finally obtains[18]

$$f_j(\theta)\approx ib_jJ_1(kb_j\theta)/\theta,\quad \theta<<(kb_j)^{-1/3}\ . \tag{15}$$

The differential cross section

$$|f_j(\theta)|^2=b_j^2[J_1(kb_j\theta)]^2/\theta^2$$

contains a central peak and smaller side lobes typical of the diffraction pattern produced by an opaque object. Most of the scattering is contained in a cone of half angle $\theta\approx 4/kb_j$.

Equation (15) is valid not only in the diffractive cone $\theta<(kb_j)^{-1}$, but also in a range $(kb_j)^{-1}<\theta<(kb_j)^{-1/3}$. Inside the diffractive cone, Eq. (15) can be approximated by

$$f_j(\theta)\approx\tfrac{1}{2}ikb_j\exp(-\tfrac{1}{8}k^2b_j^2\theta^2)\quad kb_j\theta\lesssim 1\ . \tag{16}$$

Although Eq. (16) is valid for diffractive scattering, if Eq. (16) rather than Eq. (15) is used in calculating collision rates and one-dimensional collision kernels, the results may differ by as much as 20% from the true hard-spheres values. [The results differ because the calculations require integrations in a range where Eq. (16) is not strictly valid.] Despite this discrepancy, we shall use Eq. (16) in subsequent calculations, owing to its simple analytical form. Given the spirit of this illustrative example, the slight errors which are introduced are not overly significant. For completeness, however, results using the correct amplitude (15) are given in Appendix B.

B. Population kernels

The population density in velocity space $\rho_{ii}(\vec{v},t)$ satisfies a transport-type equation in which the collision terms are of the form[3]

$$\left.\frac{\partial\rho_{ii}(\vec{v},t)}{\partial t}\right|_{\text{coll}} = -\Gamma_i(v)\rho_{ii}(\vec{v},t) + \int W_{ii}(\vec{v}'\rightarrow\vec{v})\rho_{ii}(\vec{v}',t)d\vec{v}' \ . \tag{17}$$

The first term on the right-hand side is the loss at rate $\Gamma_i(v)$ of population density $\rho_{ii}(\vec{v},t)$, while the second term gives the increase of $\rho_{ii}(\vec{v},t)$ resulting from collisions which change the velocity from $\vec{v}'$ to $\vec{v}$. The collision kernel $W_{ii}(\vec{v}'\rightarrow\vec{v})$ gives the probability density per unit time that a collision changes the active-atom velocity from $\vec{v}'$ to $\vec{v}$ and is related to the differential scattering cross section by[3]

$$W_{ii}(\vec{v}'\rightarrow\vec{v}) = Nv\,|f_i(v,\theta)|^2 v^{-2}\delta(v-v') \ , \tag{18}$$

where N is the perturber density and θ is the angle between $\vec{v}$ and $\vec{v}'$. The delta function ensures conservation of energy. The collision rate $\Gamma_i(v)$ is defined as

$$\Gamma_i(v) = \int W_{ii}(\vec{v}\rightarrow\vec{v}')d\vec{v}' \ , \tag{19}$$

which, together with Eq. (18) yields

$$\Gamma_i(v) = Nv\sigma_i(v) \ , \tag{20a}$$

where

$$\sigma_i(v) = \int |f_i(v,\theta)|^2 d\Omega_v \tag{20b}$$

is the total elastic state i scattering cross section. Equation (20) is in the standard form for a collision rate.

For hard-sphere scattering, the collision kernel, obtained from Eqs. (12), (16), and (18) is

$$W_{ii}(\vec{v}'\rightarrow\vec{v}) = Nv^{-1}\delta(v-v') \times \begin{cases} b_i^2/4, & \theta >> (kb_i)^{-1/3} \\ (k^2b_i^4/4)\exp(-\frac{1}{4}k^2b_i^2\theta^2), & \theta \lesssim (kb_i)^{-1} \ . \end{cases} \tag{21}$$

It contains a part corresponding to classical scattering for $\theta >> (kb_i)^{-1/3}$ and the quantum-mechanical contribution of diffractive scattering for $\theta < (kb_i)^{-1}$. The collision cross section, obtained from Eqs. (19)–(21) is

$$\sigma_i = 2\pi b_i^2 \ , \tag{22}$$

a well-known result for hard-sphere scattering in the high-energy limit. The classical and diffractive scattering each contribute πb_i^2 to the total cross section.[20]

It is instructive to use the optical theorem and Eq. (18) to rewrite Eq. (17) in the form

$$\left.\frac{\partial\rho_{ii}(\vec{v},t)}{\partial t}\right|_{\text{coll}} = -\tfrac{1}{2}[\Gamma_i(v)+\Gamma_i^*(v)]\rho_{ii}(\vec{v},t) + Nv^{-1}\int f_i(v,\theta)f_i^*(v,\theta)\delta(v-v')\rho_{ii}(\vec{v}',t)d\vec{v}' \ , \tag{23a}$$

where

$$\Gamma_j(v) = Nv(4\pi/ik)f_j(v,0) \tag{23b}$$

and $f(v,0)$ is a forward-scattering amplitude. In general $\Gamma_i(v)$ is complex, but, for hard-sphere scattering

$$\Gamma_i(v) = Nv(2\pi b_i^2) \tag{24}$$

is real.

C. Coherence kernel

The collisional time rate of change of the coherence density is given by[2,3]

$$\left.\frac{\partial\rho_{12}(\vec{v},t)}{\partial t}\right|_{\text{coll}} = -\tfrac{1}{2}[\Gamma_1(v)+\Gamma_2^*(v)]\rho_{12}(\vec{v},t) + \int W_{12}(\vec{v}'\rightarrow\vec{v})\rho_{12}(\vec{v}',t)d\vec{v}' \ , \tag{25}$$

where

$$W_{12}(\vec{v}'\rightarrow\vec{v}) = Nvf_1(v,\theta)f_2^*(v,\theta)v^{-2}\delta(v-v') \ . \tag{26}$$

It may be noticed that Eq. (25) may be obtained from Eq. (23) by the substitution $f_1^*(v,\theta) \rightarrow f_2^*(v,\theta)$. The "rate" $\Gamma_{12}^{\text{vc}}(v)$ associated with the

coherence kernel is defined by

$$\Gamma_{12}^{vc}(v)=\int W_{12}(\vec{v}\rightarrow\vec{v}')d\vec{v}' \tag{27a}$$

$$=Nv\sigma_{12}^{vc}(v)\ , \tag{27b}$$

where

$$\sigma_{12}^{vc}(v)=\int f_1(v,\theta)f_2^*(v,\theta)d\Omega_v\ . \tag{28}$$

For hard-sphere scattering in the classical region $\theta>>(kb_j)^{-1/3}$, the collision kernel obtained from Eqs. (26) and (12), is

$$W_{12}(\vec{v}'\rightarrow\vec{v})=Nv^{-1}(b_1b_2/4)\delta(v-v')e^{i\phi(\theta)}\ , \tag{29a}$$

where

$$\phi(\theta)=2k(b_2-b_1)\sin(\theta/2)\ . \tag{29b}$$

If $k(b_2-b_1)>>1$, as assumed,[21] $W_{12}(\vec{v}'\rightarrow\vec{v})$ varies very rapidly with $\vec{v}'$ and the integral term in Eq. (25) averages to zero. Thus, *effectively*, $W_{12}(\vec{v}'\rightarrow\vec{v})$ is zero in the classical scattering region, a conclusion reached in Sec. II using the distinct trajectory argument. On the other hand, for diffractive scattering $\theta<(kb_i)^{-1}$, the collision kernel obtained using Eqs. (26) and (16), is

$$W_{12}(\vec{v}'\rightarrow\vec{v})=\tfrac{1}{4}Nv^{-1}\delta(v-v')k^2b_1^2b_2^2 \times\exp[-\tfrac{1}{8}k^2(b_1^2+b_2^2)\theta^2]\ . \tag{30}$$

As predicted in Sec. II, the coherence kernel is nonvanishing only in the diffractive scattering domain.

Using Eqs. (27) and (30), one can derive a velocity-changing coherence cross section and rate

$$\sigma_{12}^{vc}=2\pi b_1^2b_2^2/(b_1^2+b_2^2)\ , \tag{31a}$$

$$\Gamma_{12}^{vc}(v)=Nv\sigma_{12}^{vc}\ . \tag{31b}$$

For future reference, we also define a "total" cross section σ_{12}^t and rate $\Gamma_{12}^t(v)$ by

$$\sigma_{12}^t=\tfrac{1}{2}(\sigma_1+\sigma_2)=\pi(b_1^2+b_2^2)\ , \tag{32a}$$

$$\Gamma_{12}^t(v)=Nv\sigma_{12}^t\ , \tag{32b}$$

and a phase-interrupting cross section σ_{12}^{ph} and rate $\Gamma_{12}^{ph}(v)$ by

$$\sigma_{12}^{ph}=\sigma_{12}^t-\sigma_{12}^{vc}=\pi(b_1^4+b_2^4)/(b_1^2+b_2^2)\ , \tag{33a}$$

$$\Gamma_{12}^{ph}(v)=Nv\sigma_{12}^{ph}\ . \tag{33b}$$

[The corresponding values of $W_{12}(\vec{v}'\rightarrow\vec{v})$, σ_{12}^{vc}, σ_{12}^t, and σ_{12}^{ph} obtained using the scattering amplitude (15) instead of (16) are given in Appendix B. They differ at most by $\approx 20\%$ from these values.]

D. One-dimensional coherence kernel

A situation of practical importance in laser spectroscopy involves the interaction of atoms with one or more single-mode laser fields. Assuming the fields to propagate in the $\pm z$ direction, one is led to the conclusion that, in the absence of collisions, the density-matrix element $\rho_{12}(\vec{v},t)$ may be factored as

$$\rho_{12}(\vec{v},t)=\rho_{12}(\vec{v}_t)\rho_{12}(v_z,t)\ , \tag{34}$$

where $\vec{v}_t$ is a velocity transverse to the z axis. The transverse component of the density-matrix element may be taken as constant in time since it is unaffected by the atom-field interaction. While this is no longer rigorously true when collisions occur,[22] one might still assume Eq. (34) to hold to a first approximation. In that case one can insert Eq. (34) into Eq. (25), and integrate over $\vec{v}_t$ to obtain

$$\left.\frac{\partial\rho_{12}(v_z,t)}{\partial t}\right|_{coll}=-\Gamma_{12}^t(v_z)\rho_{12}(v_z,t)+\int_{-\infty}^{\infty}W_{12}(v_z'\rightarrow v_z)\rho_{12}(v_z',t)dv_z'\ , \tag{35}$$

where the one-dimensional kernel $W_{12}(v_z'\rightarrow v_z)$ is defined as

$$W_{12}(v_z'\rightarrow v_z)=\int W_{12}(\vec{v}'\rightarrow\vec{v})\rho_{12}(\vec{v}_t')d\vec{v}_t'd\vec{v}_t\ , \tag{36}$$

and the one-dimensional total collision rate is $\Gamma_{12}^t(v)_z=\frac{1}{2}[\Gamma_1(v_z)+\Gamma_2^*(v_z)]$, where

$$\Gamma_i(v_z)=\int\Gamma_i(v)\rho_{12}(\vec{v}_t)d\vec{v}_t\ . \tag{37}$$

In addition, a one-dimensional velocity-changing coherence rate $\Gamma_{12}^{vc}(v_z)$ can be defined by

$$\Gamma_{12}^{vc}(v_z)=\int\Gamma_{12}^{vc}(v)\rho_{12}(\vec{v}_t)d\vec{v}_t=\int W_{12}(v_z\rightarrow v_z')d_z'\ . \tag{38}$$

In order to carry out the calculations implicit in Eqs. (30)–(38), we assume $\rho_{12}(\vec{v}_t)$ is described by a thermal distribution

$$\rho_{12}(\vec{v}_t)=(\pi u^2)^{-1}\exp(-v_t^2/u^2)\ , \tag{39}$$

where u is the most probable active-atom speed. Substituting Eqs. (30) and (39) into Eq. (36) and recalling that $k=mv/\hbar$, one may obtain the coherence kernel

$$W_{12}(v_z'\rightarrow v_z)=\tfrac{1}{4}N(\pi u^4)^{-1}(b_1^2b_2^2/\lambda\!\!\!^{-2})\int v\delta(v-v')\exp(-v^2\theta^2/u^2\theta_0^2)\exp(-v_t'^2/u^2)d\vec{v}_t'd\vec{v}_t\ , \tag{40}$$

where

$$\lambda\!\!\!^{-}=\hbar/u\ , \tag{41}$$

$$\theta_0^2=8\lambda\!\!\!^{-2}/(b_1^2+b_2^2)<<1\ , \tag{42}$$

$$v^2=v_t^2+v_z^2;\quad v'^2=v_t'^2+v_z'^2\ , \tag{43}$$

and

$$\cos\theta=\vec{v}\cdot\vec{v}'/v^2\ . \tag{44}$$

The integrals in Eq. (40) are not overly difficult to evaluate. Writing $d\vec{v}_t=v_t dv_t d\phi_t$ and $d\vec{v}_t'=v_t' dv_t' d\phi_t'$, one can integrate Eq. (40) over v_t' to arrive at

$$W_{12}(v_z'\rightarrow v_z)=\tfrac{1}{4}N(\pi u^4)^{-1}(b_1^2b_2^2/\lambda\!\!\!^{-2})\int_0^{2\pi}d\varphi_t\int_0^{2\pi}d\varphi_t'\int_0^{\infty}v_t dv_t v^2\exp(-v^2\bar{\theta}^2/u^2\theta_0^2)\exp(-v_t^2/u^2)\ , \tag{45}$$

where $\bar{\theta}$ is θ evaluated at $v_t'^2=v_t^2+v_z^2-v_z'^2$ and terms of order $(v_z^2-v_z'^2)/u^2$ are neglected owing to the diffractive nature of the scattering ($\bar{\theta}\lesssim\theta_0<<1$). For $\bar{\theta}<<1$, one can use Eq. (44) to obtain

$$\bar{\theta}^2=\frac{(v_z-v_z')^2}{v_t^2}+\frac{v_t^2}{v^2}(\varphi_t-\varphi_t')^2\ . \tag{46}$$

After Eq. (46) is substituted into Eq. (45), the remaining integrals can easily be evaluated to yield the coherence kernel

$$W_{12}(v_z'\rightarrow v_z)=N\sigma_{12}^{vc}\theta_0^{-1}\exp[-(v_z-v_z')^2/\theta_0^2u^2]\exp\left[\frac{-2|(v_z-v_z')v_z'|}{\theta_0u^2}\right]\left[\frac{1}{2}+\frac{v_z'^2}{u^2}+\frac{|v_z'(v_z-v_z')|}{\theta_0u^2}\right]\ , \tag{47}$$

where σ_{12}^{vc} is given by Eq. (31). In terms of dimensionless variables

$$x=(v_z-v_z')/\theta_0u\ , \tag{48a}$$

$$y=v_z'/u\approx v_z/u\ , \tag{48b}$$

Eq. (47) may be written

$$W_{12}(x,y)=N\sigma_{12}^{vc}\theta_0^{-1}e^{-x^2}e^{-2|xy|}(\tfrac{1}{2}+y^2+|xy|)\ . \tag{49}$$

The coherence kernel (47) [or (49)], is centered at $x=(v_z-v_z')/\theta_0u=0$ and has a width $|v_z-v_z'|\approx u\theta_0<<u$ if $|y|<1$. (If $|y|>>1$, the width is of order $u\theta_0/|y|$.) For $|y|=|v_z'|/u>>1$, the kernel becomes exponential. The one-dimensional coherence kernel is displayed in Fig. 3 for several values of y. It is this type of kernel that one expects to encounter in laser spectroscopy experiments.

[It is interesting to note that the kernel width remains of order θ_0u *independent* of the active-atom-to-perturber mass ratio (see discussion in Appendix A). As the perturber to active-atom mass ratio decreases, there *is* a decrease in the scattering angle as measured in the laboratory frame relative to that measured in the center-of-mass frame; however, this effect is exactly compensated by an increase in the diffractive scattering cone in the center-of-mass system [the scattering angle varies as (reduced mass)$^{-1/2}$]. Thus, the kernel width is always of order $\theta_0u\propto[m(\sigma_{12}^t)^{1/2}]^{-1}$. A low-mass active atom must be used to maximize the coherence kernel width. The fact that the kernel width increases with decreasing σ_{12}^t is reasonable; smaller obstacles produce larger diffraction cones.]

The various one-dimensional rates can also be calculated. From Eqs. (38), (49), and (31) one finds

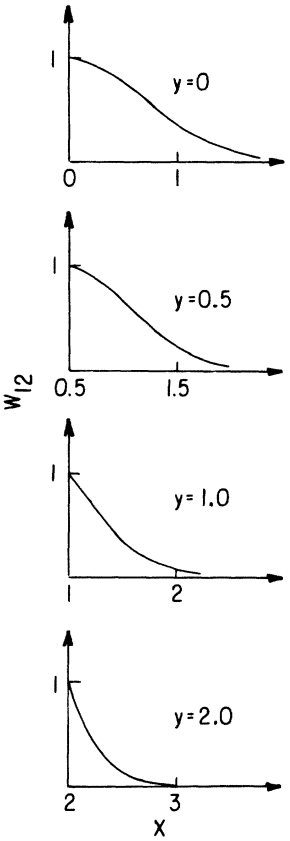

FIG. 3. One-dimensional coherence collision kernel $W_{12}(\vec{v}_z' \to \vec{v}_z)$ as a function of $x=(v_z-v_z')/\theta_0 u$ for several values of $y=v_z'/u$. The kernel is in units of $N\sigma_{12}^{vc}\theta_0^{-1}(\frac{1}{2}+y^2)$ so that $W_{12}=1$ at $x=0$. Only positive x and y are shown since $W_{12}(x,y)=W_{12}(-x,y)=W_{12}(x,-y)$.

$$\Gamma_{12}^{vc}(y)=Nu_z(y)\sigma_{12}^{vc}=Nu_z(y)\left[\frac{2\pi b_1^2 b_2^2}{b_1^2+b_2^2}\right], \tag{50}$$

where $u_z(y)$ is the value of v averaged over the transverse velocity distribution, i.e.,

$$u_z(y)=(\pi u^2)^{-1}\int d\vec{v}_t(v_t^2+y^2u^2)^{1/2}e^{-v_t^2/u^2}$$
$$=|y|+(\pi^{1/2}/2)e^{y^2}[1-\Phi(|y|)], \tag{51}$$

where Φ is the error function. From Eqs. (37), (39), (24), (51), (32), and (33), one obtains

$$\Gamma_i(y)=Nu_z(y)\sigma_i=Nu_z(y)(2\pi b_i^2), \tag{52}$$

$$\Gamma_{12}^{t}(y)=\tfrac{1}{2}[\Gamma_1(y)+\Gamma_2(y)]=Nu_z(y)\sigma_{12}^{t}$$
$$=Nu_z(y)[\pi(b_1^2+b_2^2)], \tag{53}$$

and

$$\Gamma_{12}^{ph}(y)=\Gamma_{12}^{t}(y)-\Gamma_{12}^{vc}(y)=Nu_z(y)\sigma_{12}^{ph}$$
$$=Nu_z(y)\left[\frac{\pi(b_1^4+b_2^4)}{b_1^2+b_2^2}\right]. \tag{54}$$

IV. COLLISION KERNELS IN LASER SPECTROSCOPY

It remains to determine the manner in which the collision kernels and rates modify the observables which are measured in various experiments. The reason for the success of traditional pressure-broadening theories in explaining many types of spectral line shapes will emerge naturally from this discussion.

In order to observe the effects of population kernels, the first step is to selectively excite (or deplete) a velocity subset of active atoms in state i. This selectivity can generally be achieved by using a narrow-band laser of frequency Ω to excite a transition having frequency ω. Only those atoms with velocity $v_z=(\Omega-\omega)/K$, where $\vec{K}=K\hat{z}$ is the laser propagation vector, will see a Doppler-shifted frequency that is resonant with the transition frequency. In this manner, one can excite a longitudinal velocity subset of atoms with velocities v_z centered at $(\Omega-\omega)/K$ having a width in velocity space of order $u_0=\gamma/K$, where γ is some effective width (natural plus collision) associated with the transition.

Collisions will now modify the population density only if the collision-induced velocity changes produced within the velocity-selected state's lifetime is greater than or of the order of u_0. That is, for collisions to produce noticeable effects, they must significantly alter the velocity distribution created in the excitation process. Typically, $u_0/u\simeq 0.01$, so that both large-angle and diffractive scattering can modify the population density. The population density of the velocity-selected state may be monitored by measuring the absorption of a second laser on the same or another transition containing the level in question.[2,3] Such effects have been observed using both steady-state[23] and coherent transient[14,24] techniques. It might be noted that collision-induced changes in population densities can also be measured using a standing-wave photon-echo technique.[25]

Coherence kernel

It is much more difficult to detect the velocity changes associated with the coherence kernel

$W_{12}(\vec{v}'\rightarrow\vec{v})$ than with the population kernel $W_{ii}(\vec{v}'\rightarrow\vec{v})$ owing to two factors. First, *the coherence kernel is limited to diffractive scattering,* whereas the population kernel contains a large-angle scattering component that is more easily detectable. Second, the effective lifetime for coherences is generally significantly smaller than that for populations (see discussion below); consequently, there may occur too few collisions within the coherence lifetime to produce a measurable effect. Therefore, it requires some analysis to determine the feasibility of measuring velocity changes associated with the coherence kernel.

In the rest frame of the active atom, the effect of a laser field $\vec{E}=\hat{i}E_0\cos\Omega' t$ is to produce a "coherence" $\rho_{12}(\vec{v},t)$ which essentially follows the field dependence, i.e., $\rho_{12}(\vec{v},t)=\tilde{\rho}_{12}(\vec{v},t)e^{+i\Omega' t}$.[26] The frequency Ω' seen in the atomic rest frame is equal to $\Omega-Kv_z$ for a laser field of frequency Ω and propagation vector $K=K\hat{z}$. Thus, $\rho_{12}(\vec{v},t)$ varies as

$$\rho_{12}(\vec{v},t)=\tilde{\rho}_{12}(\vec{v},t)e^{i\Omega t}e^{-iKv_z t}, \tag{55}$$

where $\tilde{\rho}_{12}(\vec{v},t)$ is generally a slowly varying function of $\vec{v}$ and t. Assuming that $\tilde{\rho}_{12}(\vec{v},t)$ can be factored as in Eq. (34), one can substitute Eq. (55) into Eq. (25) and average over $\vec{v}_t$ to obtain

$$\left.\frac{\partial\tilde{\rho}_{12}(v_z,t)}{\partial t}\right|_{\text{coll}}=-\Gamma_{12}^{t}(v_z)\tilde{\rho}_{12}(v_z,t)+\int W_{12}(v_z'\rightarrow v_z)e^{-iK(v_z-v_z')t}\tilde{\rho}_{12}(v_z',t)dv_z', \tag{56}$$

which is the analog of Eq. (35).

We wish to examine Eq. (56) as it applies to linear spectroscopy, saturation spectroscopy, and photon-echo experiments. To do so, it is useful to draw some general conclusions concerning Eq. (56). First, there is always some effective coherence lifetime τ associated with $\tilde{\rho}_{12}$ which is determined by the natural and collisional widths of the levels, as well as the width of the velocity distribution represented by $\tilde{\rho}_{12}(v_z,t)$ (τ^{-1} is approximately equal to the linewidth observed in linear spectroscopy). Second, the coherence kernel limits $|v_z-v_z'|$ to values [see Eq. (47)]

$$|v_z-v_z'|\lesssim u\theta_0\equiv\delta u<<u, \tag{57a}$$

$$\delta u=\frac{(8\pi)^{1/2}\hbar}{m(\sigma_{12}^{t})^{1/2}}. \tag{57b}$$

Consequently, if $K\delta u\tau<<1$ and if $\tilde{\rho}_{12}(v_z',t)$ is slowly varying compared with $W_{12}(v_z'\rightarrow v_z)$, the integral term in Eq. (56) may be approximated by $\Gamma_{12}^{\text{vc}}(v_z)\rho_{12}(v_z,t)$ if use is made of Eq. (38).[27] Thus, using Eq. (54), one finds

$$\left.\frac{\partial\tilde{\rho}_{12}(v_z,t)}{\partial t}\right|_{\text{coll}}=-\Gamma_{12}^{\text{ph}}(v_z)\tilde{\rho}_{12}(v_z,t), \tag{58a}$$

provided

$$K\delta u\tau<<1;$$

$$\left|\frac{1}{\tilde{\rho}_{12}}\frac{d\tilde{\rho}_{12}}{dv_z'}\right|<<\left|\frac{1}{W_{12}(v_z'\rightarrow v_z)}\frac{dW_{12}(v_z'\rightarrow v_z)}{dv_z'}\right|. \tag{58b}$$

Equation (58a) is precisely the equation used in traditional pressure-broadening theories![7,2,3]

We are let to conclude that traditional pressure-broadening theories give accurate results *provided* that Eq. (58b) is satisfied. Although the theory presented in this work and traditional pressure-broadening theories lead to the same formal result when Eq. (58b) is satisfied, the interpretation of the result is very different in the two theories. In our case, it is the separation of trajectories that leads to a destruction rate $\Gamma_{12}^{\text{ph}}(v)\approx Nvb_W^2$ is (recall b_W the Weisskopf radius), while, in traditional theories, it is large phase shifts for collisions having $b<b_W$ which destroy ρ_{12}. Thus, despite the fact that the neglect of trajectory effects cannot be justified, one is still at liberty to use the results of conventional pressure-broadening theories,[7] provided that Eq. (58b) is valid.[28] We now analyze some typical experimental situations to determine whether or not Eq. (58) can be used and to determine under what conditions the velocity changes associated with the coherence kernel may be detected.

Linear spectroscopy. In linear spectroscopy, there is no velocity selectivity and $\tilde{\rho}_{12}(v_z,t)$ is a thermal distribution having width u. The effective coherence time owing to this distribution is $\tau=(Ku)^{-1}$ at low pressure (leading to a width $\simeq\tau^{-1}\simeq Ku\simeq$Doppler width) and decreases with increasing pressure. Under these conditions, Eq. (58b) is always satisfied, implying that linear spectroscopy may be described using conventional pressure-broadening theories. The net effect of collisions is a broadening of the spectral profiles.[29]

Saturation spectroscopy. In saturation spectroscopy, one selectively excites a velocity distribution of width $u_0 \approx (\gamma_{12}+\Gamma_{12}^{ph})/K$, where γ_{12} is the natural width associated with the $1-2$ transition. The effective coherence time, determined by the natural and collisional decay of ρ_{12}, is of order $\tau=(\gamma_{12}+\Gamma_{12}^{ph})^{-1}$. Thus, the width of $\rho_{12}(v_z,t)$ compared with that of $W_{12}(v_z' \to v_z)$ is roughly equal to $(\gamma_{12}+\Gamma_{12}^{ph})/K\delta u$, which may be of order unity at low pressures ($\Gamma_{12}^{ph} < \gamma_{12}$) but grows with increasing pressure. The quantity $K\delta u\tau$ is roughly equal to $K\delta u/(\gamma_{12}+\Gamma_{12}^{ph})$, which decreases with increasing pressure. Consequently, Eq. (58b) may be marginally violated at low pressures but should be valid at pressures where $\Gamma_{12}^{ph} >> \gamma_{12}$. At low pressures, the velocity-changing effects could introduce distortions into the saturation spectroscopy line shapes.[30] In order to observe deviations from Eq. (58a), systems having large K,[31] small γ_{12}, and an active atom with low mass should be sought. An attempt to observe velocity-changing effects on optical coherences was recently carried out with Xe as the active atom.[32] Although the method used produces line shapes that are sensitive to velocity changes associated with optical coherences, the value of K (infrared transitions) and the large mass of the Xe active atoms were not ideal for observing the effect. No direct evidence of the effects of velocity-changing collisions associated with the coherence kernel was found.[32]

Photon echoes. The photon-echo experiment is described in more detail in Sec. V. It turns out that the second inequality in Eq. (58b) is always satisfied. However, as described below, it is possible to arrange the experimental conditions such that $K\delta u\tau > 1$. In this limit, Eq. (58a) is no longer valid and the photon-echo signal reflects the effects of velocity changes associated with the coherence kernel $W_{12}(v_z' \to v_z)$. Recently, the first experimental evidence of this effect on an electronic transition was reported.[10,11]

V. PHOTON ECHO

A. General features

A photon-echo experiment offers an excellent method for monitoring the coherence ρ_{12}. In the absence of collisions and spontaneous decay, the photon echo signal is formed as follows[2,9,33]:

(1) At $t=0$, a short pulse of radiation (propagation vector $\vec{K}=K\hat{z}$) creates a coherence

$$\rho_{12}(z,v_z,0)=CW(v_z)e^{-iKz},$$

where C is a constant.

(2) Between $t=0$ and $t=T$, the coherence evolves freely as

$$\rho_{12}(z,v_z,t)=CW(v_z)e^{-iKz}e^{i(\omega+Kv_z)t},$$

where ω is the transition frequency. As seen in the laboratory frame, this frequency is Doppler shifted by Kv_z. The Doppler shifts cause the dipoles to dephase relative to each other.

(3) A second short pulse at $t=T$, also having $\vec{K}=K\hat{z}$, is chosen to produce a net effect[34] of changing the sign of the $(\omega+Kv_z)$ phase factor.[2,9,33] Thus, at time $t=T$, following the second pulse,

$$\rho_{12}(z,v_z,T)=C'W(v_z)e^{-iKz}e^{-i(\omega+Kv_z)T},$$

where C' is a constant. For $t>T$, the coherence once again evolves freely as

$$\begin{aligned}\rho_{12}(z,v_z,t)&=C'W(v_z)e^{-iKz}e^{-i(\omega+Kv_z)T}e^{i(\omega+Kv_z)(t-T)}\\&=C'W(v_z)e^{-iKz}e^{i(\omega+Kv_z)(t-2T)}.\end{aligned} \tag{59}$$

The dipoles, which dephased in the period $0<t<T$, begin to rephase for $t>T$. At $t=2T$, they are all in phase an an "echo" signal is emitted. Any interference of this dephasing-rephasing process or loss of ρ_{12} owing to spontaneous decay results in a decrease in echo amplitude. Thus the photon echo serves as a sensitive probe of the coherence ρ_{12}.

Spontaneous decay results in a decrease of ρ_{12} by a factor $\exp(-\gamma_{12}t)$ and a corresponding decrease in the echo amplitude (γ_{12} is the natural width associated with the transition). The collisional time rate of change of ρ_{12} given in Eq. (35) also modifies the echo amplitude. When the effects of both spontaneous decay and collisions are incorporated into the calculation, the resulting expression for the echo amplitude produced at $t=2T$ is[9,35]

$$A(T)=\int_{-\infty}^{\infty} W(v_z)A(v_z,T)dv_z, \tag{60a}$$

where

$$A(v_z,T)=A_0\exp\left[-2\gamma_{12}T-2\Gamma_{12}'(v_z)T+2\int_0^T dt\int_{-\infty}^{\infty} dv_z'\,W_{12}(v_z'\to v_z)\cos[K(v_z-v_z')t]\right] \tag{60b}$$

is the contribution to the echo amplitude from atoms having velocity v_z.

Before specifically evaluating Eq. (60b) using the kernel (47), we can note several general features of the result (60b). The width of the coherence kernel $W_{12}(v_z' \to v_z)$ is roughly $\delta u = u\theta_0 << u$. If $K\delta uT << 1$, the velocity changes associated with the diffractive scattering region produce effects too small to be detected. In this limit, Eq. (60b) reduces to

$$A(v_z,T) \simeq A_0 \exp\{-2[\gamma_{12}+\Gamma_{12}^{\rm ph}(v_z)]T\} , \quad K\delta uT << 1 \qquad (61)$$

where Eqs. (38) and (54) have been used. For times T such that diffractive scattering effects are negligible, the loss of echo amplitude arises from spontaneous decay (γ_{12} term) and the destruction of ρ_{12} produced by the separation of trajectory effect [$\Gamma_{12}^{\rm ph}(v_z)$ term].

On the other hand, if $k\delta uT > 1$, the velocity changes associated with the diffractive scattering region lead to phase changes in ρ_{12} that are large enough to *further reduce the echo amplitude* from the value (61) produced by spontaneous decay and separation of trajectory effects. In the limit that $K\delta uT >> 1$, the integral term in Eq. (60b) averages to zero[36] and the echo amplitude becomes

$$A(v_z,T) = A_0 \exp\{-2[\gamma_{12}+\Gamma_{12}^{f}(v_z)]T\} , \quad K\delta uT >> 1 . \qquad (62)$$

The reduction of echo amplitude is now caused by spontaneous decay, separation of trajectory effects, *and* diffractive coherent scattering. The rate of echo decay, $\Gamma_{12}^{f}(v_z)$, in the long-time domain is larger than the rate $\Gamma_{12}^{\rm ph}(v_z)$ in the short-time domain.

As the pulse separation T is increased, the effects of diffractive coherence scattering on the echo amplitude become more pronounced. For $K\delta uT >> 1$, every scattering event, on average, contributes to the collisional exponential loss term appearing in Eq. (62).

One may ask why the photon-echo method is distinctly superior to saturation spectroscopy in revealing these effects since the effective coherence lifetime $\tau \simeq [\gamma_{12}+\Gamma_{12}^{\rm ph}(v_z)]^{-1}$ is the *same* in both cases. The answer to this question lies in the way in which the diffractive scattering affects the respective line shapes. In saturation spectroscopy, diffractive scattering produces corrections to *linewidths* of order $K\delta u\tau$; since $K\delta u\tau$ is generally less than unity the distortion of the line shape is usually difficult to observe. In photon-echo experiments, however, diffractive scattering produces corrections of order $k\delta uT$ which may be arbitrarily large. Of course, the effective coherence lifetime is playing a role by reducing the signal strength by a factor $\exp(-2T/\tau)$, which is much less than unity when $K\delta uT >> 1$. However, since echo signals are intrinsically large, measurements in the region where $T/\tau \lesssim 5$ are readily performed; such measurements[10,11] have led to a clear demonstration of the effects of diffractive scattering on coherences. The spectral resolution of echo signals obtained with pulse separations $T > 1/\gamma_{12}$ is less than the natural width associated with the 1—2 transition.

B. Specific evaluation of echo amplitude

The integral appearing in Eq. (60b) is

$$I = \int_{-\infty}^{\infty} dv_z' \, W_{12}(v_z' \to v_z) \frac{\sin[K(v_z - v_z')T]}{K(v_z - v_z')} . \qquad (63)$$

If the dimensionless variables $x = (v_z - v_z')/\delta u$ and $y = v_z/u \simeq v_z'/u$ given in Eq. (48) are reintroduced and the coherence kernel (49) substituted into Eq. (63), one obtains

$$I(y,\Theta) = 2N\sigma_{12}^{\rm vc} uT\Theta^{-1} \int_0^{\infty} dx \, e^{-x^2-2x|y|}(\tfrac{1}{2}+y^2+x|y|)\sin(\Theta x)/x , \qquad (64)$$

where

$$\Theta = K\delta uT = \theta_0(KuT) , \qquad (65)$$

and θ_0 is defined by Eq. (42). The integrals are tabulated[17] and one may write Eq. (64) as

$$I(y,\Theta) = Nu\sigma_{12}^{\rm vc} TY(y,\Theta) , \qquad (66)$$

where

$$Y(y,\Theta)=2\sum_{n=0}^{\infty}\left[-\frac{\Theta^2}{2}\right]^n\frac{e^{y^2/2}}{2n+1}[2^{-1/2}D_{-(2n+1)}(\sqrt{2}\,|y|)+|y|D_{-2n}(\sqrt{2}\,|y|)]\,, \tag{67}$$

and D_n is a parabolic cylinder function.[17] Combining Eqs. (60b) and (63)–(67), we obtain

$$A(yu,T)=A_0\exp\{-2[\gamma_{12}+\Gamma_{12}^t(yu)]T+2Nu\sigma_{12}^{vc}TY(y,\Theta)\}\,. \tag{68}$$

Equation (68) must now be averaged over a Maxwellian distribution in yu to arrive at the echo amplitude (60a). The integration must be done numerically. For illustrative purposes, we present two approximate methods for performing this average.

Method 1. If only a narrow range of velocities is excited by the laser pulse[37] such that $|y|<<1$, one can set $y=0$ in Eq. (68) and use Eqs. (68), (60a), (51), and (53) to obtain the echo amplitude

$$A(T)=A_0\exp(-2\{\gamma_{12}+Nu_z(0)[\sigma_{12}^t-\sigma_{12}^{vc}\Theta^{-1}\sqrt{\pi}\Phi(\Theta/2)]\}T)\,, \tag{69}$$

where Φ is the error function and $u_z(0)=u\sqrt{\pi}/2$ is the average value of v for $v_z=0$.[38] We note that

$$\ln[A(T)/A_0]\sim\begin{cases}-2[\gamma_{12}+Nu_z(0)(\sigma_{12}^{ph}+\sigma_{12}^{vc}\Theta^2/12)]T, & \Theta<<1\\ -2[\gamma_{12}+Nu_z(0)(\sigma_{12}^t-\sigma_{12}^{vc}\sqrt{\pi}/\Theta)]T, & \Theta>>1\end{cases} \tag{70}$$

and recall that $\Theta=K\delta uT$.

Method 2. If $W(v_z)$ is a Maxwellian distribution having width u, the assumption $|y|<<1$ no longer holds. As a rough approximation, however, we can average the *exponent* in Eq. (68) over y rather than the exponential. In this manner, one finds[39]

$$A(T)=A_0\exp\left[-2\left\{\gamma_{12}+N\bar{v}\left[\sigma_{12}^t-\sigma_{12}^{vc}\sum_{n=0}^{\infty}\left[-\frac{\Theta^2}{2}\right]^n\frac{1}{(2n+1)(2n+1)!!}\right]\right\}T\right]\,, \tag{71}$$

where $\bar{v}=2u/\sqrt{\pi}$ is the average speed and the sum is a representation of the generalized hypergeometric function ${}_2F_2(\frac{1}{2},1;\frac{3}{2},\frac{3}{2};-\Theta^2/4)$. For small and large Θ, Eq. (71) may be written

$$\ln[A(T)/A_0]\sim\begin{cases}-2[\gamma_{12}+N\bar{v}(\sigma_{12}^{ph}+\sigma_{12}^{vc}\Theta^2/18)]T, & \Theta<<1\\ -2[\gamma_{12}+N\bar{v}(\sigma_{12}^t-\sigma_{12}^{vc}\pi^{3/2}/2\Theta)]T, & \Theta>>1\,.\end{cases} \tag{72}$$

The results expressed by Eqs. (70) and (72) are of a quite general nature.[8] For $\Theta<<1$

$$\ln[A(T)/A_0]\sim-2\gamma_{12}T-2N\tilde{u}\sigma_{12}^{ph}T-2cN\tilde{u}\sigma_{12}^{vc}K^2(\delta u)^2T^3,\quad K\delta uT<<1 \tag{73}$$

where c is a constant and $\tilde{u}$ some effective average speed. The T^3 dependence is a signature of velocity-changing effects. For $\Theta>>1$,

$$\ln[A(T)/A_0]\sim-2\gamma_{12}T-2N\tilde{u}\sigma_{12}^tT-2c'N\tilde{u}\sigma_{12}^{vc}/K\delta u,\quad K\delta uT>>1\,, \tag{74}$$

where c' is a constant.

To isolate the effects of collisions, we define a quantity

$$B(\Theta)=-\{\ln[A(T)/A_0]+2\gamma_{12}T\}/(2N\tilde{u}\sigma_{12}^{ph}T)\,, \tag{75}$$

which will have asymptotic limits

$$B(\Theta)\sim\begin{cases}1+c(\sigma_{12}^{vc}/\sigma_{12}^{ph})\Theta^2, & \Theta<<1\\ \sigma_{12}^t/\sigma_{12}^{ph}, & \Theta>>1\,.\end{cases} \tag{76}$$

The ratio of $B(\Theta)$ in the high- and low-Θ limits is

$$\mathscr{R}=\frac{B(\Theta)(\Theta>>1)}{B(\Theta)(\Theta<<1)}=\frac{\sigma_{12}^t}{\sigma_{12}^{ph}}=\frac{(b_1^2+b_2^2)^2}{b_1^4+b_2^4}\,, \tag{77}$$

where Eqs. (53) and (54) have been used.

As a specific example, we calculate $B(\Theta)$ using the approximation (71) (for which $u=\bar{v}$) and find

$$B(\Theta)=1+\frac{2b_1^2b_2^2}{b_1^4+b_2^4}\left[1-\sum_{n=0}^{\infty}\left[-\frac{\Theta^2}{2}\right]^n\frac{1}{(2n+1)(2n+1)!!}\right]. \tag{78}$$

In Fig. 4, $B(\Theta)$ is graphed for several values of (b_1/b_2). For $\Theta>>1$, $B(\Theta)$ asymptotically approaches the ratio $\mathscr{R}$ given by Eq. (77). The ratio $\mathscr{R}=\sigma_{12}^{t}/\sigma_{12}^{\rm ph}$ vaies from 1 to 2 as (b_1/b_2) varies from 0 to 1. It should be noted that the general conclusions reached in this section are model independent. In particular, the echo amplitude varies as $\exp(-2\Gamma_{12}^{\rm ph}T)$ for short times ($K\delta uT<<1$) and as $\exp(-2\Gamma_{12}^{t}T)$ for long times ($K\delta uT>>1$).

The curves shown in Fig. 4 are in qualitative agreement with recent experimental results on photon echoes in Li perturbed by rare gases.[11] Velocity-changing effects were also observed with Na as the active atom; the Na mass is small enough to give rise to a δu large enough [Eq. (57b)] to produce $K\delta uT>1$ for the pulse separations in that experiment.[10] In a coherent transient experiment on an electronic transition of I_2,[40] only the exponential decay of the echo amplitude typical of the short-time domain was observed. The large iodine mass leads to a small δu [Eq. (57b)]; consequently; $K\delta uT$ may remain small for the time scales used in that experiment.

VI. SUMMARY

When atoms that have been created in a superposition state by a radiation field undergo elastic collisions in an atomic vapor, two distinct types of effects occur. There is a modification of both the population-velocity distributions $\rho_{ii}(\vec{v},t)$ and the coherence density $\rho_{ij}(\vec{v},t)$ $(i\neq j)$ produced by the scattering events. The processes can be characterized by collision kernels $W_{ii}(\vec{v}'\rightarrow\vec{v})$ and $W_{ij}(\vec{v}'\rightarrow\vec{v})$, respectively. In this work, we have discussed the population kernels $W_{ii}(\vec{v}'\rightarrow\vec{v})$, but have concentrated our efforts in obtaining a physical picture of the coherence kernel $W_{ij}(\vec{v}'\rightarrow\vec{v})$. To do so, we have considered a system of two-level active atoms interacting with a radiation field and undergoing collisions with perturber atoms. The collision interaction experienced by the atom in each state was assumed to differ appreciably, as is usually the case for electronic transitions.

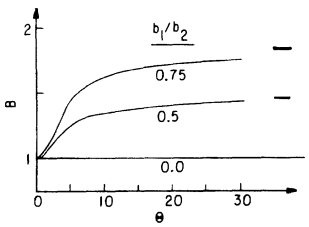

FIG. 4. Graph of $B(\Theta)$ which characterizes the photon-echo signal [Eq. (78)] as a function of $\Theta=K\delta uT$ for $b_1/b_2=0$, 0.5, 0.75. The small horizontal lines on the right side of the graph indicate the asymptotic value of $B(\Theta)$ as $\Theta\rightarrow\infty$.

Using arguments based on the uncertainty principle, we showed that collisions can be roughly divided into two regions. Collisions having an impact parameter less than some characteristic radius may be described classically, while large-impact parameter collisions, giving rise to diffractive scattering, must be treated using a quantum-mechanical approach. As a consequence of this result, the population kernel may be written as the sum of a large-scale (classical) scattering term plus a term containing the effects of diffractive scattering.

The collision-induced modifications of the atomic coherences produced by these two types of collisions are somewhat more interesting. For small-impact parameter collisions, there are distinct nonoverlapping trajectories associated with the scattering for each atomic state. Since there is no spatial overlap of states 1 and 2 following such collisions, these collisions destroy ρ_{12} and lead simply to a decay rate for ρ_{12}. Quantum mechanically, the classical separation of trajectories is represented by a rapid variation with angle of the phase of the product of the amplitudes $f_1f_2^*$. Large-impact parameter collisions, on the other hand, lead to overlapping diffractive scattering for the two states. Consequently, the coherence kernel $W_{12}(\vec{v}'\rightarrow\vec{v})$ possesses a diffractive component *only* arising from these large-impact parameter collisions. The width of the coherence kernel is effectively independent of the perturber to active-atom mass ratio.

Trajectory effects are seen to play an important role in determining the collision-induced changes

in the coherence ρ_{12}. The coherence ρ_{12} is related to the atomic polarization, which, in turn, is directly linked to the spectral properties of the medium. It seems somewhat paradoxical, therefore, that traditional pressure-broadening theories, in which separation of trajectory effects are neglected and in which collisions are assumed to affect only the phases of the optical dipoles, are so successful in describing spectroscopic line shapes. This apparent paradox was resolved in Sec. IV, where it was shown that traditional pressure-broadening may be used provided the velocity-changes associated with the coherence kernel are too small to be detectable in a given experiment. Thus, although the interpretations are different in the two approaches, the results can be identical. In linear spectroscopy, traditional pressure-broadening theory is always valid, if, as assumed, the collisional interaction differs appreciably for the two states between which the optical transition occurs. Traditional pressure-broadening theory is no longer applicable if the velocity changes associated with the diffractive coherence kernel $W_{12}(\vec{v}'\rightarrow\vec{v})$ *can* be experimentally measured. Such effects should be marginally observable in saturation spectroscopy and have been observed for the first time in photon-echo experiments.[10,11]

To illustrate various features of the problem, we adopted a simple model of hard-sphere scattering to describe the collisions. The results, however, are quite general and can be easily extended to arbitrary potentials. The hard-sphere model enabled us to obtain closed-form expressions for the various collision kernels and rates. In addition, we used the model to calculate an expression for the photon-echo amplitude, which clearly indicates the importance of velocity-changing collisions associated with $W_{12}(\vec{v}'\rightarrow\vec{v})$. If one uses a more realistic interaction potential, the resulting expressions must be evaluated numerically.

It should be noted that the semiclassical approach used in this work is valid only if the de Broglie wavelength of the atoms (in the center-of-mass reference frame) is much smaller that the characteristic Weisskopf collision radius b_W. Moreover, any effects of orbiting or of rainbow or glory scattering have been neglected. A rigorous discussion of the validity of the semiclassical approach has been given by Avrillier, Borde, Picart, and Tran Minh.[4] A calculation is in progress which is designed to determine the conditions under which our general approach to calculating the coherence kernel retains its validity.

ACKNOWLEDGMENTS

We should like to thank S. Avrillier for several discussions concerning the applicability of the semiclassical approach in calculating collision kernels and for providing copies of articles related to the subject (Ref. 4) prior to publication. P.R.B. would also like to acknowledge several meetings with S. Avrillier, J. LeGouët, N. Picart, and N. Tran Minh in which problems relating to the coherence kernel were discussed. These meetings served as a stimulus for carrying out the work presented herein. This research is supported by the U. S. Office of Naval Research (Contracts Nos. N00014-77-C-0553 and N00014-78-C-517) and by the U. S. Joint Services Electronics Program (Contract No. DAAG29-79-C-0079).

APPENDIX A

In Appendix A, the results of Sec. III are generalized to allow for an arbitrary perturber to active-atom mass ratio. The collision kernel is given by[2,3]

$$W_{ij}(\vec{v}'\rightarrow\vec{v})=N\left[\frac{m}{\mu}\right]^3\int d\vec{v}_r'\int d\vec{v}_r W_p(\vec{v}'-\vec{v}_r')\delta\left[\vec{v}_r-\vec{v}_r'-\frac{m}{\mu}(\vec{v}-\vec{v}')\right]v_r^{-1}\delta(v_r-v_r')F_{ij}(v_r',|\vec{v}_r-\vec{v}_r'|)\,. \tag{A1}$$

The quantities appearing in Eq. (A1) are the product of scattering amplitudes in the center-of-mass system

$$F_{ij}(v_r',|\vec{v}_r-\vec{v}_r'|)=f_i(v_r',|\vec{v}_r-\vec{v}_r'|)f_j^*(v_r',|\vec{v}_r-\vec{v}_r'|)\,, \tag{A2}$$

the perturber velocity distribution

$$W_p(\vec{v}_p)=(\pi u_p^2)^{-3/2}\exp(-v_p^2/u_p^2)\,, \tag{A3}$$

where u_p is the most probable perturber speed, and the reduced mass μ. Equation (A1) represents the collision kernel in the center-of-mass frame averaged over the perturber velocity distribution consistent with conservation of momentum and energy.

Integrating Eq. (A1) over $\vec{v}_r'$ and setting

$$\vec{\eta}=(m/\mu)(\vec{v}-\vec{v}') , \tag{A4}$$

one finds

$$W_{ij}(\vec{v}'\rightarrow\vec{v})=N(m/\mu)^3\int d\vec{v}_r W_p(\vec{v}'-\vec{v}_r+\vec{\eta})\delta(v_r-|\vec{v}_r-\vec{\eta}|)v_r^{-1}F_{ij}(v_r,\eta) . \tag{A5}$$

The angular integrals can be carried without too much difficulty[5,13,41] and one may obtain

$$W_{ij}(\vec{v}'\rightarrow\vec{v})=N(m/\mu)^3(2\pi)\eta^{-1}W_p(\tfrac{1}{2}\vec{\eta}+\vec{v}')\int_0^\infty q\,dq\,\exp(-q^2/u_p^2)I_0(2qv_s/u_p^2)F_{ij}((q^2+\tfrac{1}{4}\eta^2)^{1/2},\eta)) , \tag{A6}$$

where

$$v_s=(vv'/|\vec{v}-\vec{v}'|)\sin\theta , \tag{A7}$$

θ is the angle between $\vec{v}'$ and $\vec{v}$, and I_0 is a modified Bessel function.

When the exponential approximation to the scattering amplitude (16) is used, one has

$$F_{ij}(v_r,\eta)=\tfrac{1}{4}k_r^2b_i^2b_j^2\exp[-\tfrac{1}{8}k_r^2(b_i^2+b_j^2)\theta_r^2] , \tag{A8}$$

where

$$\vec{k}_r=\mu\vec{v}_r/\hbar \tag{A9}$$

and

$$\theta_r=2\sin^{-1}(\eta/2v_r) \tag{A10}$$

are the k vector and scattering angle, respectively, in the center-of-mass frame. Substituting Eqs. (A8)–(A10) into (A6) and assuming $\theta_r<<1$ (diffractive scattering region), we find

$$W_{ij}(\vec{v}'\rightarrow\vec{v})=\frac{N}{\sqrt{\pi}}\left[\frac{m}{\mu}\right]^3\frac{b_i^2b_j^2\exp[-\eta^2/(\theta_0^r u_r)^2]}{4\lambda\!\!\!^{-2}_r u_p\eta}\exp\left[-\left[\frac{\eta}{2}+\frac{\vec{v}'\cdot\vec{\eta}}{\eta}\right]^2\frac{1}{u_p^2}\right]u_r^{-2}[v'^2+\tfrac{1}{4}\eta^2+u_p^2-(\vec{v}'\cdot\vec{\eta}/\eta)^2] , \tag{A11}$$

where

$$\vec{\eta}=(m/\mu)(\vec{v}-\vec{v}') ,$$

$$\lambda\!\!\!^{-}_r=\hbar/\mu u_r , \tag{A12}$$

$$u_r^2=u^2+u_p^2 , \tag{A13}$$

and

$$(\theta_0^r)^2=8\lambda\!\!\!^{-2}_r/(b_i^2+b_j^2)<<1 . \tag{A14}$$

The various collision rates defined by Eqs. (19), (27), (32), and (33) are easily calculated starting from Eq. (A1). One finds

$$\Gamma_i(v)=Nu_r(v)(2\pi b_i^2) , \tag{A15a}$$

$$\Gamma_{12}^t(v)=Nu_r(v)[\pi(b_1^2+b_2^2)] , \tag{A15b}$$

$$\Gamma_{12}^{vc}(v)=Nu_r(v)\left[\frac{2\pi b_1^2b_2^2}{b_1^2+b_2^2}\right] , \tag{A15c}$$

$$\Gamma_{12}^{\rm ph}(v)=Nu_r(v)\left[\frac{\pi(b_1^4+b_2^4)}{b_1^2+b_2^2}\right], \tag{A15d}$$

where $u_r(v)$ is the active-atom perturber relative speed averaged over the perturber velocity distribution, i.e.,

$$\begin{aligned} u_r(u_p z)&=\int W_p(\vec{v}_p)\,|\,\vec{v}-\vec{v}_p\,|\,d\vec{v}_p \\ &=\pi^{-1/2}u_p e^{-z^2}[1+2\pi^{1/2}z^{-1}(1+2z^2)e^{z^2}\Phi(z)]\,, \end{aligned} \tag{A16a}$$

with

$$z=v/u_p\,. \tag{A16b}$$

[Note that as $u_p\to 0$ and $\mu\to m$, one regains the results of Sec. III. If $u\to 0$, and $\mu\to m_p$ (perturber mass), $W_{12}(\vec{v}'\to\vec{v})\sim\Gamma_{12}^{\rm vc}(v)\delta(\vec{v}-\vec{v}')$, and $u_r(u_p z)\sim u_r(0)=2\pi^{-1/2}u_p$.]

To obtain the one-dimensional kernel, one multiplies Eq. (A1) by $W(\vec{v}_t')$ and integrates over $\vec{v}_t$ and $\vec{v}_t'$. The resulting integrals can be reduced to a triple integral[5,13,41] of the form

$$W_{ij}(v_z'\to v_z)=4\pi^{-1/2}\beta\kappa\int_0^\infty ds_t\int_0^\infty dq\int_{-\infty}^\infty dp\,e^{-\beta^2(p-y)^2}\exp[-\kappa^{-1}(q^2+q_0^2)]F_{12}((q_0^2+p^2+q^2)^{1/2},\,\eta)\,, \tag{A17}$$

where

$$\beta=u/u_p=(m_p/m)^{1/2}\,, \tag{A18}$$

$$\kappa=(1+\beta^2)/\beta^2\,, \tag{A19}$$

$$\vec{s}=(\vec{v}-\vec{v}')/u=\vec{s}_t+s_z\hat{z}\,, \tag{A20}$$

$$q_0^2=s_t^{-2}(\tfrac{1}{2}\kappa s^2+ps_z)^2\,, \tag{A21}$$

and

$$y=v_z'/u\,. \tag{A22}$$

With the kernel given by the exponential approximation (A8), Eq. (A17) may be integrated to give

$$\begin{aligned} W_{12}(v_z'\to v_z)=&\tfrac{1}{2}N\sigma_{12}^{\rm vc}(\theta_0^r)^{-1}e^{-\beta^2x^2} \\ &\times\{[\tfrac{1}{2}+\beta^{-2}+y^2+x\bar{y}(1-\beta^{-2})-x^2]e^{-2x\bar{y}}[1+\Phi(\bar{y}-x)] \\ &+[\tfrac{1}{2}+\beta^{-2}+y^2-x\bar{y}(1-\beta^{-2})-x^2]e^{2x\bar{y}}[1-\Phi(\bar{y}+x)]+2\pi^{-1/2}xe^{-\bar{y}^2}e^{-x^2}\}\,, \end{aligned} \tag{A23}$$

where

$$x=|\,v_z-v_z'\,|/(\beta u\theta_0^r)\,, \tag{A24}$$

$$y=v_z'/u\,,$$

$$\bar{y}=\beta y=v_z'/u_p\,, \tag{A25}$$

$$\theta_0^r=\kappa\theta_0\,. \tag{A26}$$

The kernel (A23) reduces to Eq. (49) in the limit $\beta\to\infty$ and has a width of order $\theta_0 u$ for $|\,y\,|\lesssim 1$. For $\beta<<1$ and $|\,y\,|\lesssim 1$, the effective width of the kernel is of order $\beta\theta_0^r u=\kappa\beta\theta_0 u=(1+\beta^2)^{1/2}\theta_0 u\approx\theta_0 u$. Thus, *regardless of the ratio of perturber to active-atom mass ratio,* the kernel width (for $|\,y\,|\lesssim 1$) is of order

$$\begin{aligned} u\theta_0&=2\sqrt{2}\hat{\lambda}u/(b_1^2+b_2^2)^{1/2} \\ &=2(2\pi)^{1/2}\hbar/m\,(\sigma_{12}^t)^{1/2}\,. \end{aligned} \tag{A27}$$

This somewhat surprising result arises from the cancellation of two effects. As m_p/m (or β) decreases, there is an *increase* in the size of the diffraction cone in the center-of-mass system [recall that $\theta_r\propto(\mu u_r)^{-1}$

$=(1+\beta^{-2})^{1/2}\theta_0]$. This effect is compensated by a *decrease* in the scattering angle as measured in the laboratory frame. Thus, the collision width depends primarily on the active-atom mass and total collision cross section.

In Fig. 5, the kernel

$$W_{12}(0\rightarrow\beta u\theta_0^r x)=N\sigma_{12}^{vc}(\theta_0^r)^{-1}e^{-\beta^2x^2}\{(\tfrac{1}{2}+\beta^{-2}-x^2)[1-\Phi(x)]+\pi^{-1/2}xe^{-x^2}\} \tag{A28}$$

is plotted as a function of

$$(1+\beta^2)^{1/2}x=v_z/u\theta_0=v_z/\delta u \tag{A29}$$

for several values of β. The $\beta=0.1$ and $\beta=10$ curves correspond to asymptotic limits of the kernel for the cases $\beta<<1$ and $\beta>>1$ respectively; thus the kernel width is seen to vary only slightly with β. In practice, σ^t normally increases with increasing β, implying a corresponding decrease in the kernel width. Smaller collision cross sections produce a larger diffractive-scattering cone.

The various one-dimensional rates are still given by Eqs. (A15) if one replaces v by v_z and $u_r(v)$ by $u_z(v_z)$, where $u_z(v_z)$ is the relative speed averaged over the perturber and transverse active-atom velocity distributions, i.e.,

$$u_z(v_z)=\int W(\vec{v}_t)W_p(\vec{v}_p)\,|\,\vec{v}-\vec{v}_p\,|\,d\vec{v}_p d\vec{v}_t\ , \tag{A30}$$

where

$$\vec{v}=\vec{v}_t+v_z\hat{z}\ .$$

Explicitly,[41] one finds

$$u_z(uy)=u_p\left[\beta y\Phi(\beta y)+\pi^{-1/2}e^{-\beta^2y^2}\left[1+\pi^{1/2}\int_0^\infty dx\,e^{-x^2/\kappa^2\beta^2}\cosh(2yx/\sqrt{\kappa})[1-\Phi(x/\kappa\beta^2)\right]\right]\ . \tag{A31}$$

APPENDIX B

In Appendix B, we derive expressions for the various collision kernels and rates using the amplitude (15) for hard-sphere scattering instead of its exponential approximation (16). Moreover, the cross sections are also calculated directly using Eq. (11) to illustrate the origin of the distinct trajectory approximation $k(b_2-b_1)>>1$.

Using Eqs. (A2) and (15), we find

$$F_{ij}(v_r,\eta)=b_ib_j\theta_r^{-2}J_1(k_rb_i\theta_r)J_1(k_rb_j\theta_r)\ , \tag{B1}$$

where θ_r is given by Eq. (A10). If Eq. (B1) is substituted into Eq. (A6) and the assumption $\theta_r<<1$ is used, one may obtain [cf. Eqs. (A11)–(A14)]

$$W_{ij}(\vec{v}'\rightarrow\vec{v})=\frac{N}{\sqrt{\pi}}\left[\frac{m}{\mu}\right]^3\frac{b_ib_ju_r^2}{u_p\eta^3}J_1\left[\frac{b_i\eta}{u_r\lambda\!\!\!^{-}_r}\right]J_1\left[\frac{b_j\eta}{u_r\lambda\!\!\!^{-}_r}\right]$$

$$\times\{\exp[-(\tfrac{1}{2}\eta+\vec{v}'\cdot\vec{\eta}/\eta)^2/u_p^2]\}u_r^{-2}[v'^2+\tfrac{1}{4}\eta^2+u_p^2-(\vec{v}'\cdot\vec{\eta}/\eta)^2]\ , \tag{B2}$$

where $\vec{\eta}=(m/\mu)(\vec{v}-\vec{v}')$. Equation (B2) reduces to Eq. (A11) if $b\eta/u_r\lambda\!\!\!^{-}_r<<1$.

The rate obtained from Eqs. (27), (A1), and (B1) is

$$\Gamma_{ij}^{vc}(v)=Nu_r(v)\int d\Omega_r b_ib_j\theta_r^{-2}J_1(k_rb_i\theta_r)\times J_1(k_rb_j\theta_r)\ , \tag{B3}$$

where $u_r(v)$ is given by Eq. (A16). If $k_r(b_2-b_1)>>1$, the θ_r integral can be replaced by an integral from 0 to ∞. In that case, for $b_2>b_1$, one finds[17]

$$\Gamma_{ij}^{vc}(v)=Nu_r(v)(\pi b_i^2)\quad b_i\leq b_j\ . \tag{B4}$$

Thus, the various cross sections and rates defined in Eqs. (19) and (31)–(33) are given by $(b_2>b_1)$

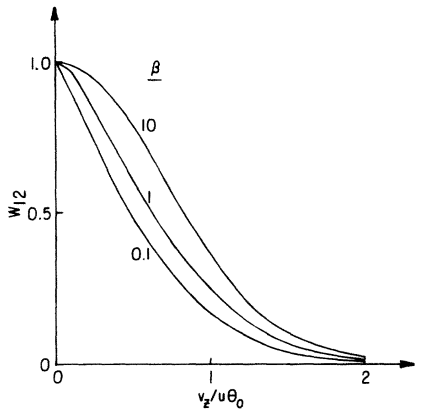

FIG. 5. Graphs of the one-dimensionel kernel $W_{12}(0\rightarrow v_z)$ as a function of $(1+\beta^2)^{1/2}x=v_z/u\theta_0$ for several values of $\beta=u/u_p=(m_p/m)^{1/2}$. Notice that the width of the kernel is essentially independent of β, although its shape changes somewhat. The kernel is in units of $N\sigma_{12}^{vc}(\theta_0^r)^{-1}$ and is normalized such that $W_{12}(0\rightarrow 0)=1$.

$$\sigma_i=2\pi b_i^2 , \tag{B5a}$$

$$\sigma_{12}^{vc}=\pi b_1^2 , \tag{B5b}$$

$$\sigma_{12}^{t}=\pi(b_1^2+b_2^2) , \tag{B5c}$$

$$\sigma_{12}^{ph}=\pi b_2^2 , \tag{B5d}$$

and $\Gamma(v)=Nu_r(v)\sigma$. The cross section σ_{12}^{vc} can differ by as much as 17% from that calculated using the exponential approximation to the scattering amplitude [see Eq. (31)].

Integral expressions for the one-dimensional kernels and rates can be easily obtained using Eqs. (36), (39), (A1), (B1), and (27). Without explicitly writing expressions for these quantities, we note that for large enough $|\vec{v}-\vec{v}'|$ or $|\vec{v}_z-\vec{v}_z'|$, it is possible for the population kernel to have side lobes and for the coherence kernel to go negative (the exponential approximation always gives a positive kernel). This feature is already seen in Eq. (B2). Near the "center" of the kernel, $|v_z-v_z'|<u\theta_0$, the exponential approximation (16) produces a collision kernel that has the same form as the one calculated using the correct amplitude (15).

To finish this appendix (and article), we calculate σ_{12}^{vc} directly from Eq. (11) without using the assumption that $k(b_2-b_1)>>1$. Using the definition

$$\sigma_{ij}^{vc}=\mathrm{Re}\int f_i(\theta)f_j^*(\theta)d\Omega \tag{B6}$$

along with Eq. (11) for $f_i(\theta)$, one easily derives

$$\sigma_{ij}^{vc}=4\pi k^{-2}\sum_{l=0}^{\infty}(l+\tfrac{1}{2})[\,2\sin^2\eta_l^{(1)}\sin^2\eta_l^{(2)}+\tfrac{1}{2}\sin(2\eta_l^{(1)})\sin(2\eta_l^{(2)})] , \tag{B7}$$

where

$$\eta_l^{(i)}=\tan^{-1}[j_l(kb_i)/n_l(kb_i)] \tag{B8}$$

is the state-i hard-sphere scattering phase shift. Using the properties of the spherical Bessel functions,[17] one can show that $\eta_l^{(i)}\sim 0$ exponentially for $l<L_i$ so that the $\cos(2\eta_l^i)$ terms average to zero. One is left with

$$L_i=kb_i \tag{B9}$$

(assuming $b_i<b_j$). Equation (B7) may be rewritten as

$$\sigma_{ij}^{vc}=2\pi k^{-2}\sum_{l=0}^{L_i} l[\,1-\cos(2\eta_l^{(i)})-\cos(2\eta_l^{(j)})+\cos(\eta_l^{(j)}-\eta_l^{(i)})] . \tag{B10}$$

Again, using the properties of the Bessel functions,[17] one can show that the η_l^i are large for $l<L_i$ so that the $\cos(2\eta_l^i)$ terms average to zero. One is left with

$$\sigma_{ij}^{vc}=4\pi k^{-2}\sum_{l=0}^{L_i} l\sin^2[(\eta_l^{(j)}-\eta_l^{(i)})/2] . \tag{B11}$$

For $i=j$, Eqs. (B9) and (B11) yield $\sigma_i=2\pi b_i^2$, the quantum-mechanical result for high-energy hard-sphere scattering. For $i\neq j$, one can approximate[17]

$$\eta_l^{(2)}-\eta_l^{(1)}=l(\psi_2-\psi_1)-l(\tan\psi_2-\tan\psi_1) , \tag{B12}$$

where

$$\psi_i=\cos^{-1}(l/L_i) .$$

Since $l/L_i<<1$ for most l in the sum,

$$\psi_i-\tan\psi_i\simeq\frac{\pi}{2}-\frac{l}{2L_i}-\frac{L_i}{l} ,$$

such that

$$\eta_l^{(2)}-\eta_l^{(1)}\approx -k(b_2-b_1)+\frac{l^2}{2}\frac{(b_2-b_1)}{kb_1b_2} . \tag{B13}$$

Combining Eqs. (B13) and (B11) and changing the

sum to an integral, one finally obtains

$$\sigma_{12}^{vc}=\pi b_1^2+\frac{4\pi b_1 b_2}{k(b_2-b_1)}\sin\left[\frac{kb_1(b_2-b_1)}{4b_2}\right]\times\cos\left[\frac{k(b_2-b_1)(4b_2-b_1)}{4b_2}\right]. \quad \text{(B14)}$$

If $b_2=b_1$, $\sigma_{12}^{vc}=2\pi b_1^2$, but for $k(b_2-b_1)>>1$, $\sigma_{12}^{vc}\simeq\pi b_1^2$, in agreement with the result (B5b) derived *from diffractive scattering only.* Thus, if $k(b_2-b_1)>>1$, diffractive scattering only contributes to the coherence kernel.

---

[1]The perturber atoms are assumed to be nonreactive and simply provide an effective scattering potential which is different for states 1 and 2 of the active atom.

[2]P. R. Berman, Adv. At. Mol. Phys. 13, 57 (1977), and references therein.

[3]P. R. Berman, Phys. Rep. 43, 101 (1978).

[4]S. Avrillier, C. J. Borde, J. Picart, and N. Tran Minh, in *Proceedings of the 5th International Conference on Spectral Line Shapes,* edited by B. Wende (de Gruyter, Berlin, 1981), and (unpublished).

[5]S. Avrillier, Doctorat D'Etat thesis, University of Paris, North, 1978 (unpublished).

[6]An attempt to explain the coherence kernel for the magnetic substates of a given level has been given recently. See, J. L. LeGouët and P. R. Berman, Phys. Rev. A 24, 1831 (1981).

[7]See, for example, R. G. Breene, Jr., *The Shift and Shape of Spectral Lines* (Pergamon, New York, 1961); M. Baranger, in *Atomic and Molecular Processes,* edited by D. R. Bates (Academic, New York, 1962), Chap. 13; H. R. Griem, in *Plasma Spectroscopy* (McGraw-Hill, New York, 1964), Chap. 4; J. T. Jeffries, *Spectral Line Formation* (Blaisdell, Waltham, Massachusetts, 1968); I. I. Sobelman, *Introduction to the Theory of Atomic Spectra* (Pergamon, New York, 1972); S. Y. Chen and M. Takeo, Rev. Mod. Phys. 29, 20 (1957); J. Cooper, *ibid.* 39, 167 (1967).

[8]For a discussion of this effect (often referred to as "Dicke narrowing") [R. H. Dicke, Phys. Rev. 89, 872 (1953)], see P. R. Berman, Appl. Phys. (Germany) 6, 283 (1975), Sec. 5 and references therein.

[9]P. R. Berman, J. M. Levy, and R. G. Brewer, Phys. Rev. A 11, 1668 (1975); B. Comasky, R. E. Scotti, and R. L. Shoemaker, Opt. Lett. 6, 45 (1981).

[10]T. W. Mossberg, R. Kachru, and S. R. Hartmann, Phys. Rev. Lett. 44, 73 (1980).

[11]R. Kachru, T. J. Chen, T. W. Mossberg, S. R. Hartmann, and P. R. Berman, Phys. Rev. Lett. 47, 902 (1981).

[12]See, e.g., M. S. Child, *Molecular Collision Theory* (Academic, London, 1974), Chaps. 1–5.

[13]Population kernels of this type are discussed in A. P. Kolchenko, S. G. Rautian, and A. M. Shalagin, Nucl. Phys. Inst. Semiconductor Phys. Internal Report (unpublished).

[14]M. Gorlicki, A. Peuriot, and M. Dumont, J. Phys. Lett. (Paris) 41, L275 (1980).

[15]Equation (8) is strictly true only for smoothly varying potentials for which the impulse approximation may be used. For hard-sphere scattering, condition (8) is replaced by $k(b_2-b_1)>>1$.

[16]The stationary phase method is valid only if $kb_j\theta^3>>1$. This result may be obtained by using the asymptotic expansion

$$P_l(\cos\theta)\sim\cos[(l+\tfrac{1}{2})\theta-\pi/4]$$

and an approximation form for the phase shifts

$$\eta_l=(l+\tfrac{1}{2})(\beta-\tan\beta)-\pi/4\ ,$$

valid for $kb_j>>1$ [the angle β is defined by $\cos\beta=(l+\frac{1}{2})/kb_j$]. The net phase appearing in Eq. (11) becomes

$$\phi=-(l+\tfrac{1}{2})(\theta-2\beta+2\tan\beta)+\pi/4\ .$$

The point of stationary phase is given by $(l+\frac{1}{2})=kb_j\cos(\theta/2)$ (classical result). If $kb_j\theta^3<1<<kb_j\theta$, then the phase ϕ is a linear function of l and there is no point of stationary phase (equivalently, the third derivative term neglected in the stationary phase method is not negligible). Consequently, Eq. (12) is valid in the range $\theta>>(kb_j)^{-1/3}$, which is more limited than $\theta>>(kb_j)^{-1}$.

[17]I. S. Gradshteyn and I. M. Ryzhik, *Tables of Integrals, Series,and Products* (Academic, New York, 1965).

[18]There is no point of stationary phase provided $kb_j\theta^3<<1$, (see Ref. 16). This condition limits the range of validity of Eq. (15).

[19]If, for $\theta<<1$, one expands $P_l(\cos\theta)$ as

$$\{J_0(x)+(\theta^2/4)[(2x)^{-1}J_1(x)-J_2(x)+\tfrac{1}{6}xJ_3(x)]\}$$

(see Ref. 17), the leading correction to Eq. (14) can be shown to be of order

$$k^2b_j^2\theta^4<<(kb_j)^{-2/3}<<1\ ,$$

where the first inequality follows from the condition stated in Ref. 18.

[20]In integrating the classical contribution over solid angle, one must exclude a region $\theta<(kb_i)^{-1/3}$. This exclusion leads to corrections of order $(kb_i)^{-2/3}<<1$.

[21]For a smoothly varying potential, the condition

$k(b_2-b_1)>>1$ would be replaced by Eq. (8).

[22]For example, if atoms having a large v_z are selected, collisions can transfer some of this "heat" to the transverse velocities.

[23]C. Bréchignac, R. Vetter, and P. R. Berman, J. Phys. Lett. (Paris) 39, L231 (1978); Phys. Rev. A 17, 1609 (1978); P. F. Liao, J. E. Bjorkholm, and P. R. Berman, *ibid.* 21, 1927 (1980).

[24]T. W. Hänsch, I. S. Shahin, and A. L. Schawlow, Phys. Rev. Lett. 27, 707 (1971); J. Brochard and P. Cahuzac, J. Phys. B 9, 2027 (1976); P. Cahuzac and X. Drago, Opt. Commun. 24, 63 (1978); T. W. Mossberg, A. Flusberg, R. Kachru, and S. R. Hartmann, Phys. Rev. Lett. 42, 1665 (1979).

[25]R. Kachru, T. W. Mossberg, E. Whittaker, and S. R. Hartmann, Opt. Commun. 31, 223 (1979); T. W. Mossberg, R. Kachru, E. Whittaker, and S. R. Hartmann, Phys. Rev. Lett. 43, 851 (1979); see also J. L. LeGouët and P. R. Berman, Phys. Rev. A 20, 1105 (1979), and references therein.

[26]We assume that $|\Omega'-\omega|/(\Omega'+\omega)<<1$, where ω is the transition frequency ("rotating-wave" or resonance approximation).

[27]Owing to the narrow width of the coherence kernel, one can interchange v_z and v_z' at will.

[28]If the condition $k_r b_W >> 1$ is violated [see Eq. (A9) for the definition of k_r] owing to a very small perturber to active-atom mass ratio (e.g., electron perturbers), then the neglect of trajectory effects can be justified. However, if $k_r b_W >> 1$ as is assumed in this work, a unified picture of the collisions mechanism is achieved only when trajectory effects are incorporated into the theory.

[29]For scattering potentials other than hard sphere, collisions usually produce a shift as well as a broadening of the profiles.

[30]J. L. LeGouët and P. R. Berman, Phys. Rev. A 17, 52 (1978). In this paper, an approximation for the coherence kernel, similar in spirit to the one derived in this work, was used.

[31]Actually, it is combinations of the K's for the various transitions which enter (see Refs. 2 and 3).

[32]P. Cahuzac, J. L. LeGouët, P. E. Toschek, and R. Vetter, Appl. Phys. (Germany) 20, 83 (1979).

[33]See, for example, I. D. Abella, N. A. Kurnit, and S. R. Hartmann, Phys. Rev. 141, 391 (1966); M. Scully, M. J. Stephen, and D. C. Burnham, *ibid.* 171, 213 (1968); S. R. Hartmann, Sci. Am. 218, 32 (1968); C. H. Wang, C. K. N. Patel, R. E. Slusher, and W. J. Tomlinson, Phys. Rev. 179, 294 (1969); R. L. Shoemaker, in *Laser and Coherence Spectroscopy,* edited by J. T. Steinfeld (Plenum, New York, 1978), p. 197; T. W. Mossberg, R. Kachru, S. R. Hartmann, and A. M. Flusberg, Phys. Rev. A 20, 1976 (1979).

[34]For simplicity, we take the pulse to be resonant with the atomic transition, i.e., $K=\omega/c$.

[35]A. Flusberg, Opt. Commun. 29, 123 (1979).

[36]A somewhat more careful evaluation of Eq. (60b) in the limit $K\delta u T >> 1$ gives

$$A(v_z,T)=\exp\{-2[\gamma_{12}+\Gamma_{12}'(v_z)]T + 2\pi K^{-1}W_{12}(v_z\rightarrow v_z)\}\ .$$

The last term follows from Eq. (60b) if

$$\int_0^T \cos[K(v_z-v_z')t]dt$$

is replaced by $\pi K^{-1}\delta(v_z-v_z')$.

[37]A smooth Fourier-transform-limited pulse of duration $\Delta\tau$ excites a velocity bandwith $\Delta v_z \approx (K\Delta\tau)^{-1}$. If $\Delta\tau$ is chosen such that $Ku<\Delta\tau<<T$, only a fraction of the Maxwellian distribution is excited.

[38]Taking $y=0$ in Eq. (49) implies a Gaussian kernel. Equation (69) agrees with a related calculation (Ref. 9) in which a Gaussian kernel was used.

[39]Rather than directly averaging the exponent in Eq. (68), it is easier to perform the averaging in the exponent of Eq. (60b).

[40]R. G. Brewer and A. Z. Genack, Phys. Rev. Lett. 36, 959 (1976).

[41]P. F. Liao, J. E. Bjorkholm, and P. R. Berman, Phys. Rev. A 21, 1927 (1980), Appendix. Note that a factor of 2 is missing in the second term in the exponent in Eq. (A4) of this reference and that, in Eq. (A8), one should replace $\sqrt{2}$ by $\sqrt{\pi}$.